



# Effect of Post-weld Heat Treatment on the Microstructure and Mechanical Properties of 2.25Cr-1Mo-0.25V Ultra-Thick Steel Plate

Yanyang Wu<sup>1,4</sup> · Zongye Ding<sup>1,2,3</sup> · Wenquan Lu<sup>1</sup> · Jingchao Hou<sup>4</sup> · Qiaodan Hu<sup>1</sup> · Jianguo Li<sup>1</sup>

Received: 6 October 2023 / Revised: 2 December 2023 / Accepted: 18 December 2023 / Published online: 3 April 2024  
© The Chinese Society for Metals (CSM) and Springer-Verlag GmbH Germany, part of Springer Nature 2024

## Abstract

Ensuring the homogeneous and excellent mechanical properties of 2.25Cr-1Mo-0.25V ultra-thick steel plate is the key to the production of hydrogenation reactor equipment. Thus, it is required to understand the heterogeneity of microstructures and properties of ultra-thick plate after heat treatment. In this work, the effect of post-weld heat treatment (PWHT) on the strength, plasticity, toughness and microstructures of the 193-mm-thick steel plate was investigated, and the formation mechanism of heterogeneity was elucidated. The PWHT decreased the room- and high-temperature yield strength (YS) and ultimate tensile strength (UTS) of the steel plate after normalizing and tempering (NT), while the room- and high-temperature YS and UTS decreased from the surface to the center of 193-mm-thick steel plate. It was attributed to the enhanced decomposition of martensite–austenite (M–A) constituents and coarsening of grains and precipitated carbides.

**Keywords** Cr–Mo steel · Ultra-thick steel plate · Microstructure · Mechanical properties · Heterogeneity

## 1 Introduction

The 2.25Cr-1Mo-0.25V steel has been widely used in the petrochemical pressure vessels, heat exchanger pipes and hydrogen equipment, due to its high-temperature strength, creep resistance, hydrogen corrosion resistance and hydrogen embrittlement [1, 2]. The high content of V alloying elements and the complexity of its manufacturing process makes it necessary to conduct post-weld heat treatment (PWHT) on the welded structure after rolling the steel plate

into and welding to a cylindrical shell. The PWHT can improve the microstructure and mechanical properties of the welded joint, eliminate the welding stress, enhance the corrosion resistance, decrease the generation and propagation of cracks and further prevent the brittle failure in the welded structure [3–7]. Therefore, the simulated PWHT is crucial to ensure the standard manufacturing of the 2.25Cr-1Mo-0.25V steel pressure vessel.

Effect of PWHT on the microstructure and mechanical properties of the as-welded 2.25Cr-1Mo-0.25V steel has been investigated to provide references for the service integrity of the equipment. Li et al. [8] found that PWHT of 705 °C × 8 h increased the impact toughness of the as-welded 2.25Cr-1Mo-0.25V steel and changed the microstructure composed of granular bainite in the steel. The enhanced properties were attributed to the decomposition from martensite–austenite (M–A) constituents into carbides. Li et al. [9] determined the microstructure consisted of granular bainite and lath bainite in the 2.25Cr-1Mo-0.25V steel before and after PWHT. The PWHT promoted the widening of the bainite–ferrite lath and precipitation of coarsened carbides, decreasing the impact toughness and strength. With increasing PWHT time, the toughness and strength decreased. In addition, the PWHT decreased the residual stress and dislocations in the as-welded specimen, accompanied by the decreasing microhardness and increasing elongation and Charpy impact value [10, 11]. Consequently,

Available online at <http://link.springer.com/journal/40195>.

✉ Zongye Ding  
dingzongye@sjtu.edu.cn

✉ Qiaodan Hu  
qdhu@sjtu.edu.cn

<sup>1</sup> Shanghai Key Laboratory of Materials Laser Processing and Modification, School of Materials Science and Engineering, Shanghai Jiao Tong University, Shanghai 200240, China

<sup>2</sup> State Key Laboratory of Advanced Special Steel, Shanghai University, Shanghai 200444, China

<sup>3</sup> School of Mechatronic Engineering and Automation, Foshan University, Foshan 528225, Guangdong, China

<sup>4</sup> WuYang Iron and Steel, Wugang 450000, Henan, China

the PWHT had a strong influence on the microstructure and mechanical properties of the 2.25Cr-1Mo-0.25V steel. In practice, the 2.25Cr-1Mo-0.25V steel plate for manufacturing pressure vessel has ultra-thickness larger than 160 mm, which usually exhibits the heterogeneous microstructures from the surface to the center of ultra-thick plate and limits the manufacture of 2.25Cr-1Mo-0.25V steel pressure vessel [12]. However, the previous studies focus on the PWHT conducted on the specimen with small dimension and/or a part of the ultra-thick plate. The effect of PWHT on the heterogeneous microstructures and properties of the 2.25Cr-1Mo-0.25V steel ultra-thick plate is still unclear, as well as the formation of heterogeneity.

In this study, the effect of Min and Max PWHT on the microstructures, room- and high-temperature mechanical properties of the 2.25Cr-1Mo-0.25V steel plate with the thickness of 193 mm was investigated. The diversified microstructures and properties versus different parts of ultra-thick steel plate after PWHT were discussed, and the transition mechanism of microstructures and properties from the surface to the center of ultra-thick steel plate was elucidated. This result will provide theoretical and technical guidance for the production of 2.25Cr-1Mo-0.25V ultra-thick steel plate and pressure vessel.

## 2 Experimental

### 2.1 Materials

The raw materials were pig iron and scrap steel. The large ingot of 2.25Cr-1Mo-0.25V steel, used for manufacturing hydrogenation reactors in the petrochemical and coal chemical industries, was produced by the electric furnace smelting, ladle furnace refining, vacuum degassing and electroslag remelting. After casting, the ingot was rough rolled and finish rolled to plate, and the final rolling temperature was set to be higher than 950 °C. The chemical composition of the 2.25Cr-1Mo-0.25V steel was detected by spark atomic emission spectrometry, and the results are listed in Table 1.

### 2.2 Post-welding Heat Treatment

The 2.25Cr-1Mo-0.25V steel plate with thickness of 193 mm after normalizing (950 °C×5 h) and tempering (690 °C×2.5 h) was subjected to Min PWHT in a heating furnace at 705 °C for 8 h and Max PWHT at 705 °C for 32 h. The schematic diagram of normalizing, tempering and PWHT is shown in Fig. 1. Both of the heating and cooling rates were

set to 60 °C/s. To investigate the effect of normalizing temperature/time and tempering temperatures on the microstructures and mechanical properties of the steel plate, the normalizing temperatures were set to 920 °C and 960 °C, the normalizing times were set to 80 min and 160 min and the tempering temperatures were 680 °C, 700 °C and 720 °C, respectively.

### 2.3 Mechanical Properties Tests

To investigate the effect of PWHT on the microstructures and properties of the 2.25Cr-1Mo-0.25V steel plate at different positions, the specimen with dimension of 300 mm×200 mm×15 mm for mechanical properties tests and microstructures characterization was cut from the surface, quarter position and half position of ultra-thick plates, as shown in Fig. 2a–c. To measure the yield strength (YS), ultimate tensile strength (UTS) and elongation, the specimens with 10-mm diameter and 50-mm length were tested on an Instron Universal 1251 Testing Machine according to GB/T228.1-2010 standard. The V-notched specimens for Charpy impact test was prepared to assess the impact toughness by using ZBC2452 impact testing machine. The uniaxial tensile tests were conducted on a SHIMADZU AG-I 250 kN testing machine at various temperatures (200 °C, 250 °C, 300 °C, 350 °C, 400 °C, 450 °C, 500 °C and 550 °C) with loading rate of 1 mm/min. To keep the temperature homogeneity, the specimens were held at the desired temperatures for 6 min.

### 2.4 Microstructures Characterization

The metallographic specimens, extracted from the top surface to the center of the ultra-thick steel plate, were machined to determine the microstructures. The specimens were ground with grinding papers and mirror polished, then etched by a 5% Nital solution and cleaned with

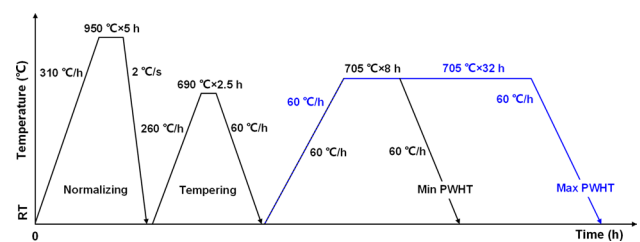
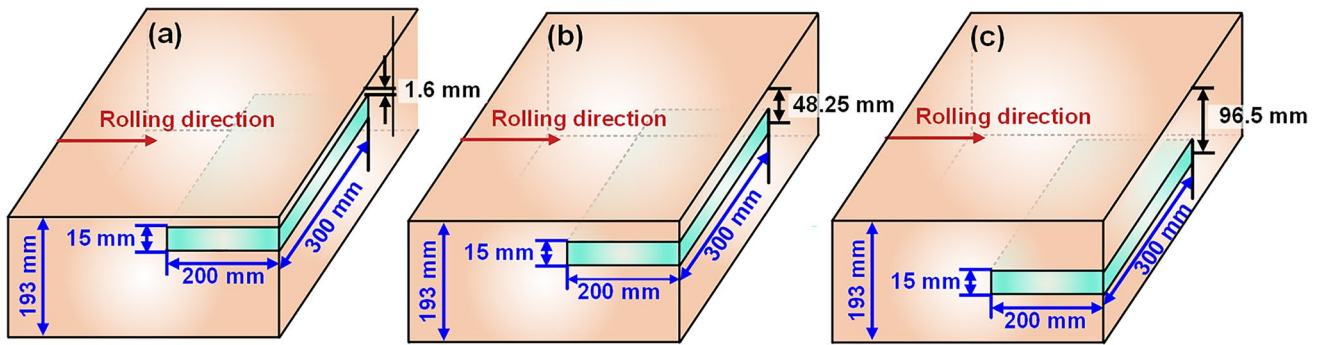


Fig. 1 PWHT of the 2.25Cr-1Mo-0.25V steel plate for different durations and cooling strategies

**Table 1** Chemical composition of the 2.25Cr-1Mo-0.25V steel plate (wt%)

C	Si	Mn	P	S	Cr	Mo	Ni	V	Cu
0.14	0.08	0.54	0.003	0.002	2.25–2.5	1.0–1.1	0.08	0.28–0.35	0.08



**Fig. 2** Positions of the specimens extracted from the ultra-thick plate and schematic diagram of the tensile and impacted samples: **a** on the surface, **b** at the quarter position, **c** at the half position

ethanol. Finally, the microstructure was characterized by using the optical microscopy (OM) and scanning electron microscopy (SEM), the morphologies of carbides were observed by using the transmission electron microscopy (TEM).

### 3 Results

#### 3.1 Phase Transformation Temperature

The continuous cooling transformation (CCT) diagram is one of the theoretical basis to formulate heat treatment process. The continuous cooling experiments in this study were conducted on the German quenching deformation

dilatometer DIL805A, and the CCT diagram was established by plotting the phase transition points at different cooling rates. The specimens were heated to 940 °C with a heating rate of 15 °C/s, held for 600 s and cooled to room temperature at cooling rates varying from 0.1 to 150 °C/s. The CCT diagram of 2.25Cr-1Mo-0.25V steel is shown in Fig. 3. The austenitizing start temperature ( $A_{c1}$ ) and finish temperature ( $A_{c3}$ ) were determined to be 794 °C and 896 °C, respectively. The proeutectoid ferrite, bainite and martensite transformation occurred during continuous cooling, instead of pearlite transformation. When the cooling rate was less than 0.5 °C/s, the austenite transformed into ferrite and bainite, the microstructure contained ferrite and bainite. When the cooling rate was between 0.5 and 8 °C/s, the austenite transformed into bainite. As the cooling rate was larger than 8 °C/s, the martensite transformation occurred,

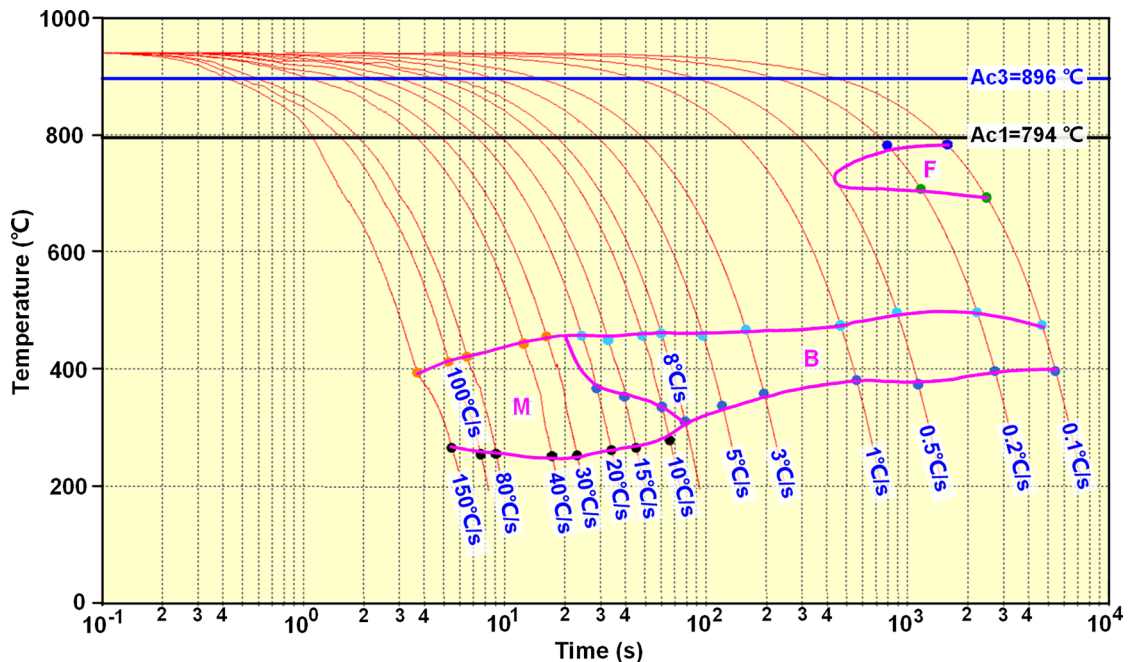


**Fig. 3** CCT diagram of 2.25Cr-1Mo-0.25V steel

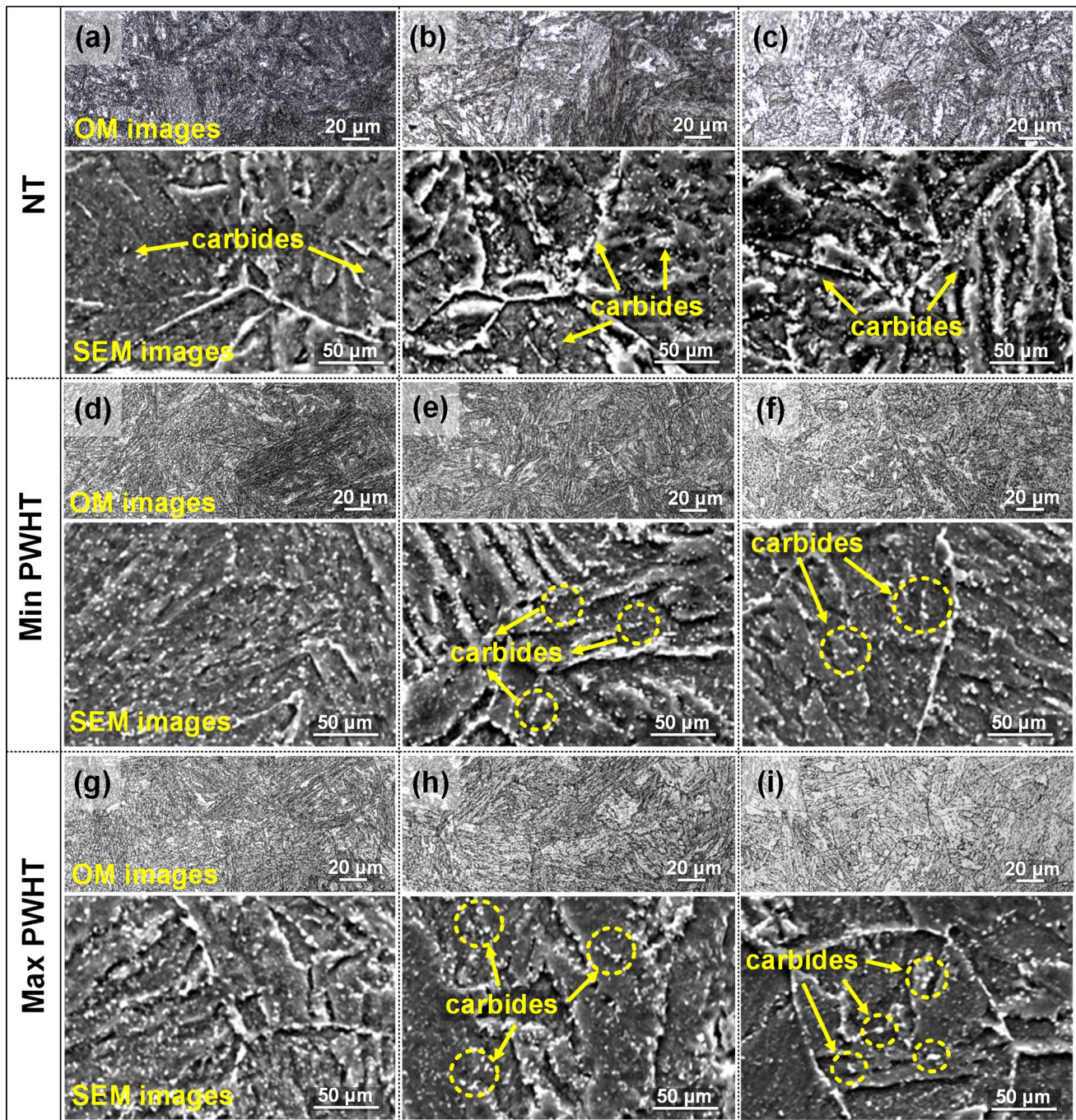


**Fig. 4** OM and SEM images of microstructures of 2.25Cr-1Mo-0.25V steel plate at different positions after without PWHT **a–c**, Min PWHT **d–f** and Max PWHT **g–i**: on the surface **a, d, g**, at the quarter position **b, e, h** and at the half position **c, f, i**

the microstructure at room temperature was consisted of bainite and martensite. When the cooling rate was larger than 30 °C/s, the single martensite existed in the microstructure. Consequently, the normalizing temperature, tempering temperature and PWHT temperature were determined to be 950 °C, 690 °C and 705 °C.

### 3.2 Microstructures After PWHT

To investigate the effect of Min PWHT and Max PWHT on the microstructures of the 2.25Cr-1Mo-0.25V steel and detect the microstructure homogenization in the 193-mm-thick plate, the OM images and magnified SEM images of

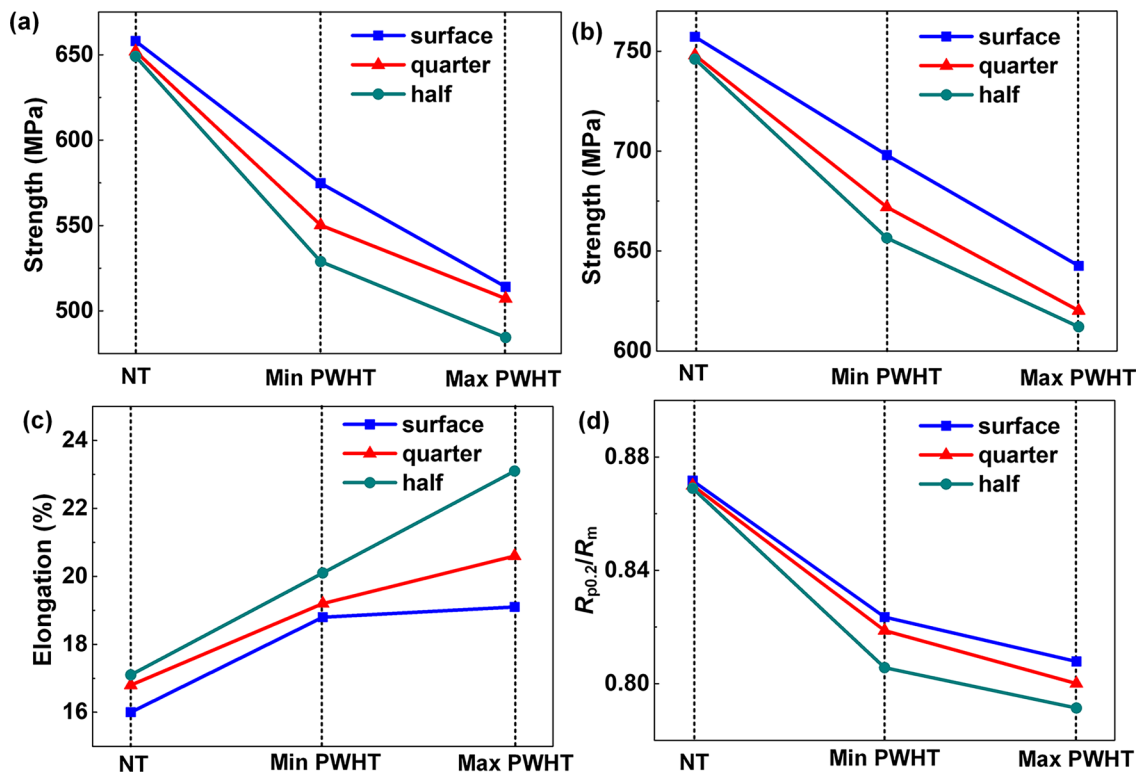


**Fig. 5** Tensile strength and plasticity of the specimens at various positions of the 2.25Cr-1Mo-0.25V ultra-thick steel plate: **a** YS, **b** UTS, **c** elongation, **d**  $R_{p0.2}/R_m$

the microstructure at different positions of the ultra-thick plate are shown in Fig. 4. The microstructures on the surface, quarter position and half position of the plate after normalizing and tempering (NT) are illustrated in Fig. 4a-c. In the OM images, the striped ferrite was formed in the granular bainite. The dimension of granular bainite in the specimens after PWHT was larger than that after NT. Additionally, the bainite size increased with increasing distance from the surface into the center of the ultra-thick plate. Based on the SEM images, the microstructure was determined to be consisted of tempering granular bainite, and carbides particles locating in the grains and on the grain boundaries. From the surface to the center of the plate, the grain size decreased and the amount of precipitated carbides increased. This was attributed to the long tempering times, promoting the precipitation of carbides. After Min PWHT and Max PWHT, the precipitation of carbides increased, especially for the carbides in the grains (Fig. 4d-i). The dimension of the carbides decreased from the surface to the half position of the steel plate. The carbides after Max PWHT was coarser than the carbides after Min PWHT. It was ascribed to the long tempering time, promoting the coarsening of the precipitated particles.

### 3.3 Mechanical Properties After PWHT

The tensile properties of different parts of the 193 mm-thick 2.25Cr-1Mo-0.25V steel plates after NT, Min PWHT and Max PWHT are shown in Fig. 5. Compared to the specimens after NT, the YS, UTS and  $R_{p0.2}/R_m$  of the specimens after PWHT decreased (Fig. 5a, b and d) and the elongation increased (Fig. 5c). The strength and  $R_{p0.2}/R_m$  after Min PWHT were larger than that after Max PWHT, while the elongation after Min PWHT was smaller. In addition, the YS, UTS and  $R_{p0.2}/R_m$  decreased from the surface, quarter position to half position of the ultra-thick steel plate. Conversely, the elongation tended to increase with increasing distance from the surface of the steel plate. The high strength of the specimens after NT, Min PWHT and Max PWHT was attributed to solid solution strengthening enhanced by the addition of alloying elements and precipitation strengthening of carbides. The PWHT and longer holding time at the quarter and half positions decreased the solution of alloying elements and promoted the precipitation of carbides, resulting in the decreased strength and increased elongation.

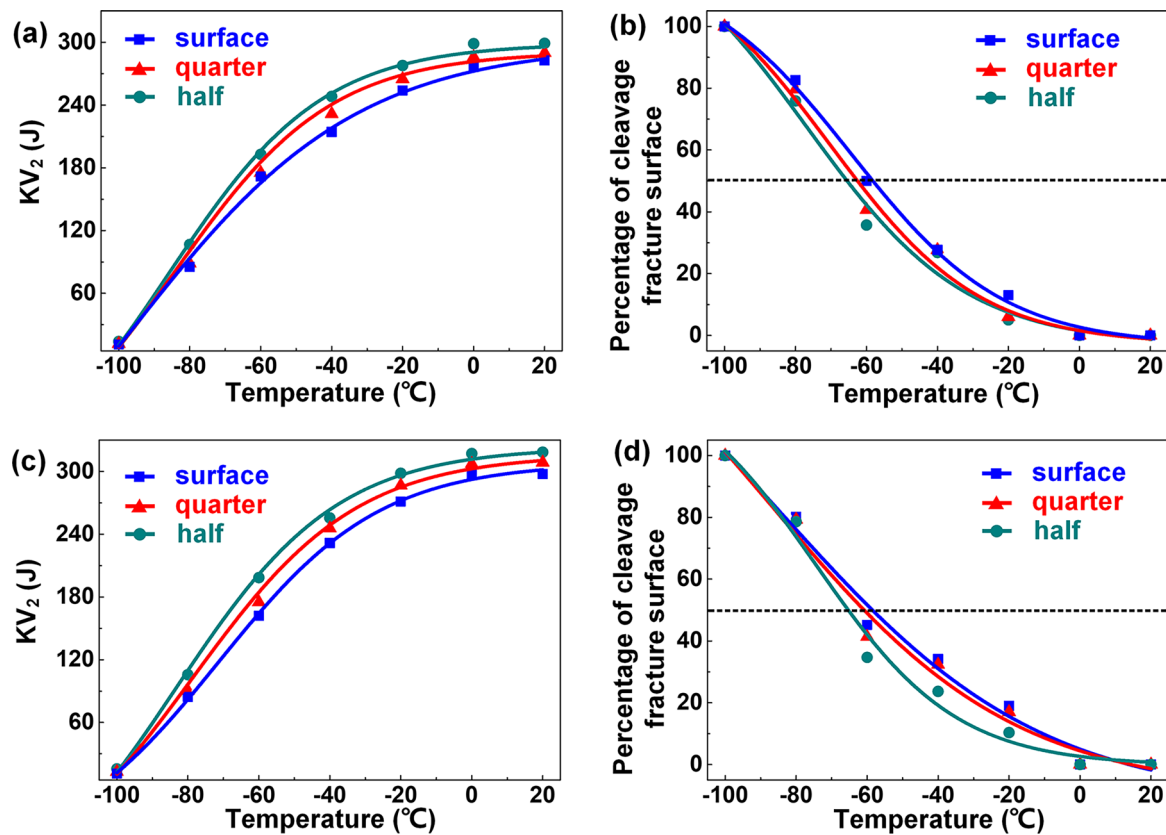


Fig. 6 Impact work and fracture percentage of the specimens versus temperature after Min PWHT a, b and Max PWHT c, d

Figure 6 shows the results of Charpy tests. The Charpy impact energies of the specimens after Min PWHT and Max PWHT increased monotonically with increasing temperature, as shown in Fig. 6a and c. The impact energy after Max PWHT was higher than that after Min PWHT, and the impact energy increased from the surface, quarter position to half position of the ultra-thick steel plate. The fracture appearance transition temperature (FATT), indicating 50% percentage of cleavage fracture surface, was determined from the curve of percentage of cleavage fracture surface and fracture morphologies of Charpy specimens (Fig. 6b and d). The FATT after PWHT decreased from the surface, quarter position to the half position.

### 3.4 Effect of Normalizing and Tempering

The YS, UTS and elongation of the specimens at the half position of the thick steel plate after NT and Max PWHT with different normalizing and tempering parameters are illustrated in Fig. 7, and the corresponding microstructures are shown in Fig. 8. For the specimens normalized

at 920 °C for 80 min, the YS and UTS increased with increasing tempering temperatures. The elongation first decreased, and then increased (Fig. 7a-c). After normalizing, the microstructure was consisted of bainite and martensite-austenite (M-A) constituents. During tempering and PWHT, the carbides precipitated from the bainite, and the M-A constituents transformed to bainite and ferrite. The amount of M-A constituents transformation and precipitated carbides increased with increasing tempering temperature (Fig. 8a-c). When the normalizing time prolonged to 160 min, the YS and UTS of specimens first increased, then decreased with increasing tempering temperature (Fig. 7). The increasing tempering time improved the strength, which was related to the decreased M-A constituents and increased carbides precipitation (Fig. 8d-f). When the normalizing temperature increased, the grains became larger and the carbides became coarser, accompanied by the enhanced precipitation of carbides on the ferrites (Fig. 8g-l). This led to the decreased strength and decreased elongation.

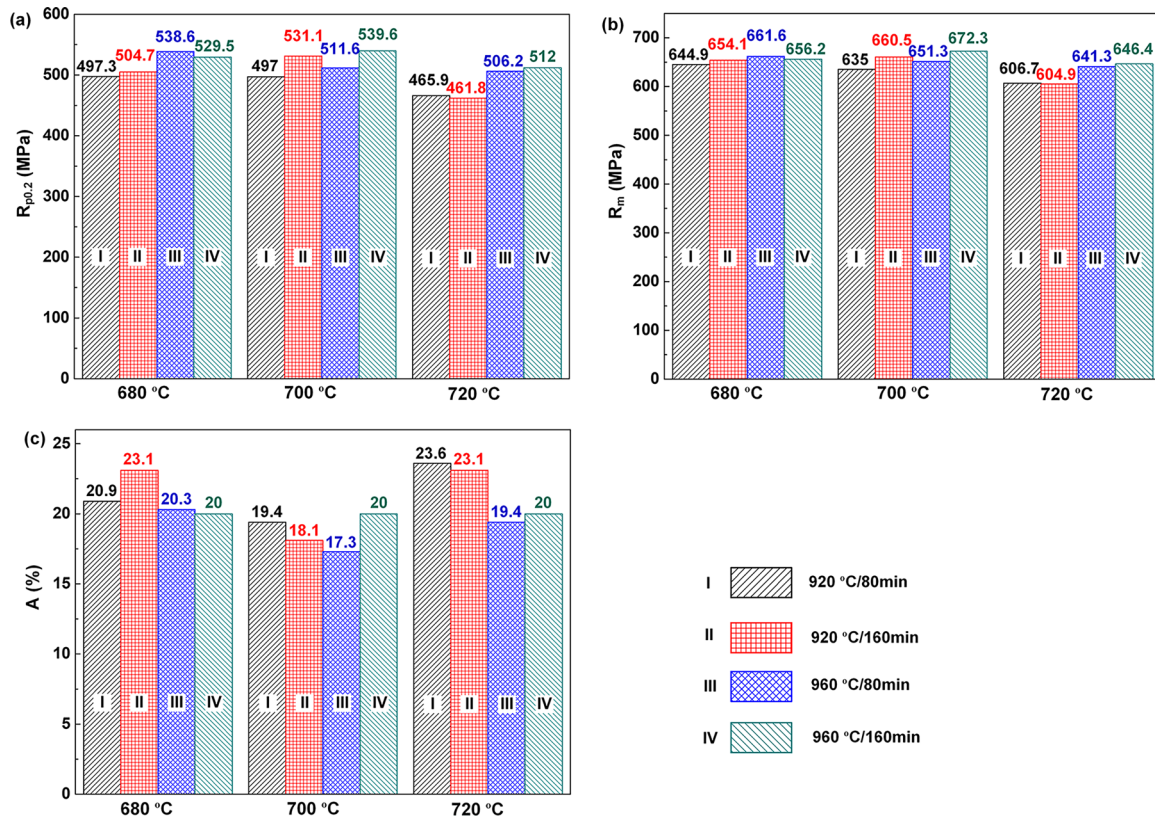


Fig. 7 Mechanical properties of the 2.25Cr-1Mo-0.25V steel after Max PWHT with different NT parameters

### 3.5 High-Temperature Properties

Figure 9 shows the variation of YS, UTS and elongation of the different parts of the ultra-thick steel plate after Min PWHT and Max PWHT versus temperatures. The YS and UTS decreased (Fig. 9a and b), while the elongation increased with increasing temperature (Fig. 9c and d). The strength after Min PWHT was higher than that after Max PWHT, while the elongation after Max PWHT was larger. It was attributed to the enhanced decomposition of M–A constituents and the coarsening of the grains and carbides with increasing PWHT time at higher temperatures. Additionally, the strength of the specimens at elevated temperatures on the surface was higher than that at the quarter position and half position. When the temperature was higher than 450 °C, the strength of different parts of the thick steel plate tended to be equal. This was ascribed to the similar decomposition of M–A constituents and the coarsening of the grains and

carbides in the different specimens at the elevated temperatures higher than 450 °C.

## 4 Discussion

Figure 10a shows the TEM image of the microstructure after NT and Max PWHT. The microstructure was consisted of bainite–ferrite, M–A constituents and carbides (Fig. 10a). The carbides were located in the grains and at the grain boundaries, and the morphologies of carbides were diversified and irregular. Jiang et al. have investigated the NT Cr–Mo–V steel and concluded that the carbides after short tempering time consisted of the agglomerated  $M_3C$  carbides and tiny needle-like VC carbides. The increased tempering time promoted the formation of rod-shaped  $M_7C_3$  and spherical  $M_{23}C_6$  carbides [13]. Based on the analysis of composition (Fig. 10b), the carbides were determined as agglomerated  $M_3C$ , rod-shaped  $M_7C_3$ ,

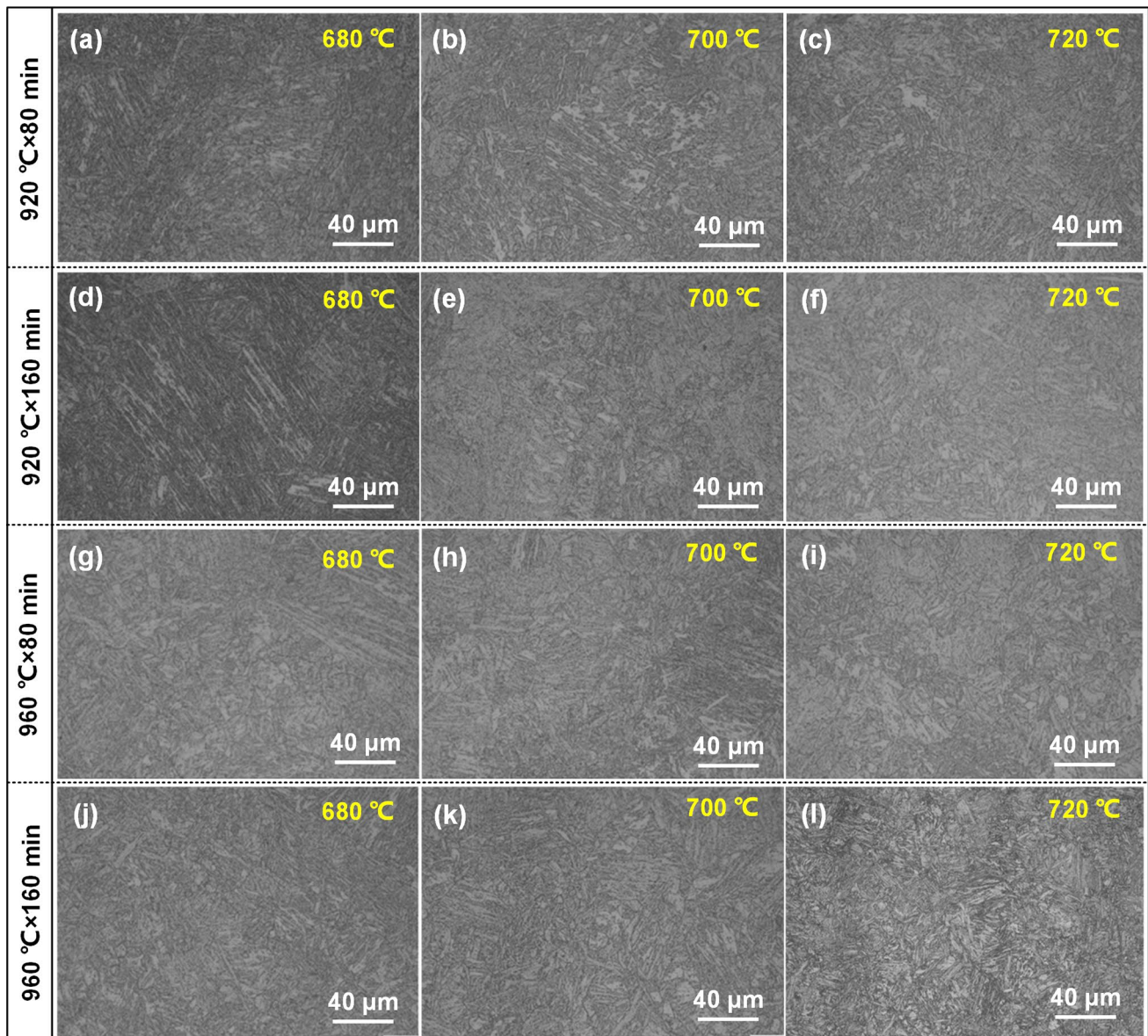
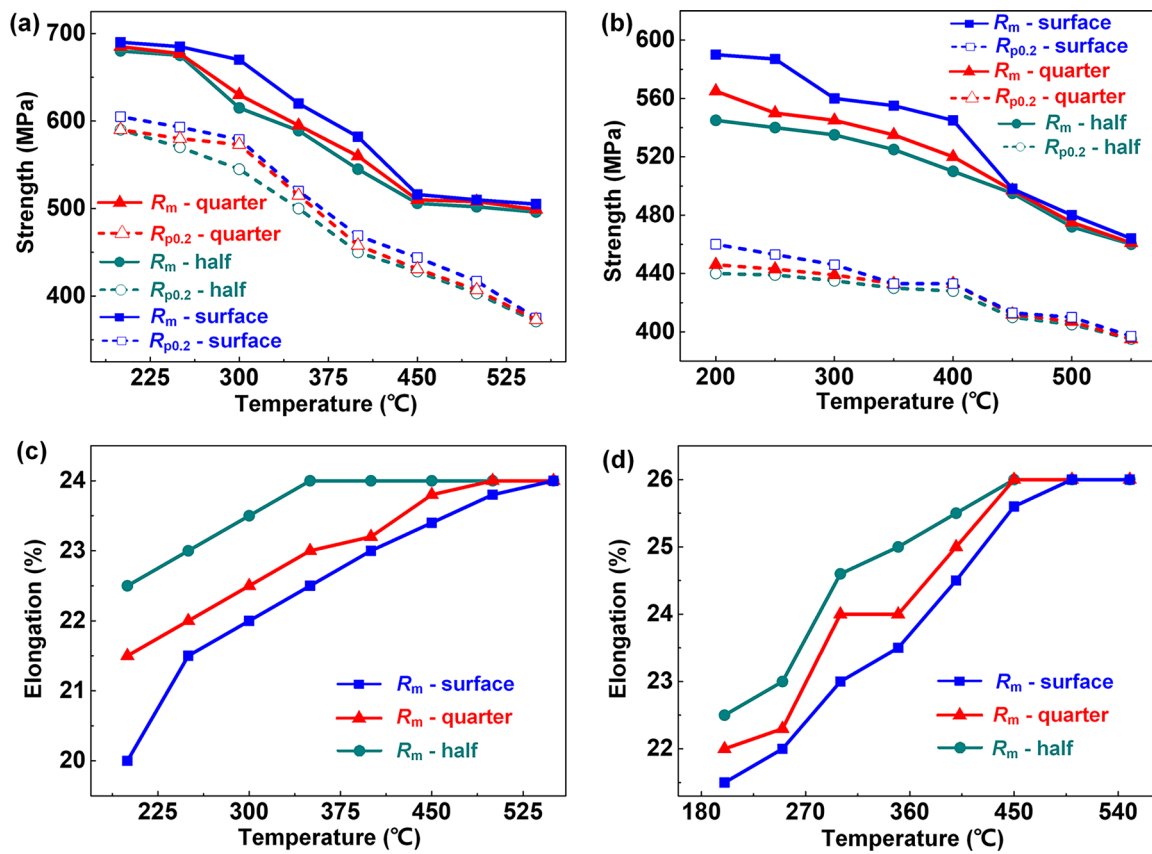


Fig. 8 Microstructures of the 2.25Cr-1Mo-0.25V steel after Max PWHT with various NT parameters

spherical  $M_{23}C_6$  and fine VC alloy carbides. This result was consistent with the samples after NT in the previous study [14]. Figure 10c shows the schematic diagram of microstructure evolution of the different parts of the ultrathick steel plate. After normalizing, the formed bainite microstructure was consisted of bainitic ferrite matrix and M–A constituents. During tempering, the M–A constituents decomposed and the carbides precipitated. The

strength of the specimens after NT was attributed to the solute strengthening and precipitate strengthening. The solute strengthening of the 2.25Cr-1Mo-0.25V steel is mainly contributed by the solution of C, Cr, Mo and V alloying elements into the matrix, resulting in the lattice distortion [15]. The corresponding strength increment ( $\Delta\sigma_{ss}$ ) was described by  $\Delta\sigma_{ss} = G(|\delta| + \frac{1}{20})|\eta|^{\frac{2}{3}}(\frac{x_0}{3})^{\frac{1}{2}}$ , where  $G$  is the shear modulus,  $\delta$  and  $\eta$  are parameters related to





**Fig. 9** High-temperature properties of the 193 mm-thick 2.25Cr-1Mo-0.25V steel plates at different positions after Min PWHT **a, c** and Max PWHT **b, d**

the lattice and shear modulus changes of the steel and  $x_a$  is the atomic percentage of solute atoms in the bainite–ferrite matrix [16]. The fine precipitated carbides strengthened the steel through hindering the dislocation motion, enhancing the precipitate–dislocation interactions [17]. The increasing strength ( $\Delta\sigma_{os}$ ) based on Orowan strengthening mechanism was determined by  $\Delta\sigma_{os} = \frac{0.81Gb}{2\pi(1-\nu)^{1/2}} \frac{\ln(2r/b)}{\lambda-2r}$ , where  $G$  is the shear modulus,  $b$  is the Burgers vector,  $\nu$  is the Poisson's ratio,  $d_p$  is the average size of carbides,  $f_v$  is the precipitated carbides volume fraction and  $\lambda$  is the spacing between the carbides [18]. The cooling rates of different specimens on the surface, quarter position and half position of the ultra-thick steel plate were diversified, reflecting the various tempering times. The long tempering time at the half position

decreased the solution of alloying elements and promoted the precipitation of carbides, resulting in the decreased YS and UTS. During PWHT, the M–A constituents continuously decomposed and the carbides precipitated in the grains and at the grain-boundaries, accompanied by the coarsening of grains and carbides. Therefore, the strength after Min PWHT and Max PWHT decreased, and the specimens at different positions exhibited diversified YS, UTS and elongation. With increasing PWHT time and distance from the surface of ultra-thick steel plate, the coarsening of grains and carbides was enhanced, further decreasing the YS and UTS of the specimens. In contrast, the toughness of the specimens after PWHT was improved with increasing distance from the surface to the half of ultra-thick plate.

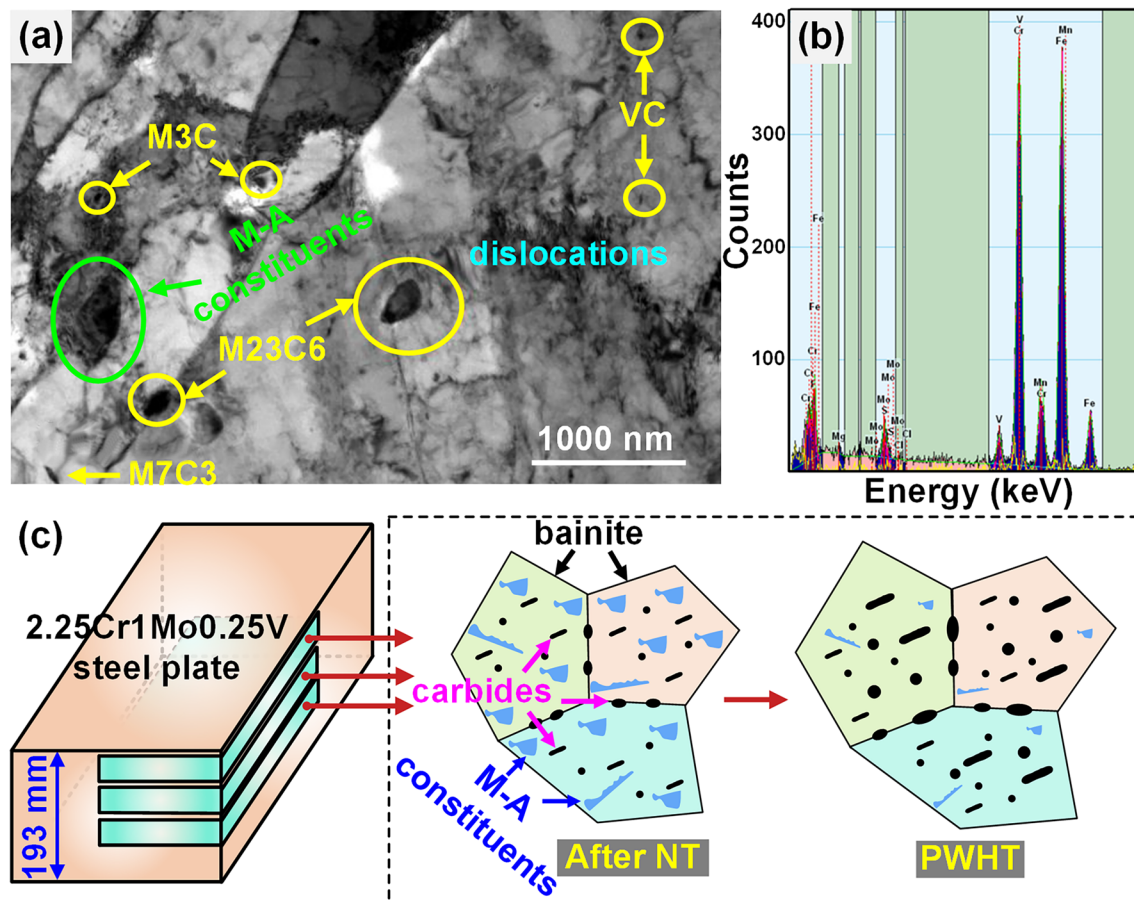


**Fig. 10** **a** TEM image and **b** compositional analysis of the microstructure of the specimens after NT and Max PWHT **c** schematic diagram of microstructure evolution of the specimens after NT and PWHT

## 5 Conclusions

The effect of PWHT on the microstructure evolution and mechanical properties of the 2.25Cr-1Mo-0.25V steel after NT was investigated, and the homogeneity of microstructure and properties of the 193 mm-thick steel plate after Min PWHT and Max PWHT was discussed. The main conclusions are as follows:

1. The microstructure of the specimens after NT consisted of bainite, ferrite matrix and M–A constituents. The PWHT promoted the decomposition of M–A constituents and coarsening of grains and precipitated carbides, decreasing the strength and increasing the elongation of steel plate after NT.
2. The YS and UTS after NT and PWHT were attributed to solute strengthening and precipitate strengthening, which decreased with increasing tempering temperatures and time. The YS and UTS after Min PWHT were

higher than Max PWHT. The 2.25Cr-1Mo-0.25 V steels after NT, Min PWHT and Max PWHT had excellent comprehensive mechanical properties.

3. The specimens at different positions exhibited heterogeneous microstructure and mechanical properties of the ultra-thick plate. The YS and UTS at RT and HT decreased, while the elongation increased from the surface, quarter position to half position, which was related to the combined effect of weakening solution strengthening, enhanced decomposition of M–A constituents and precipitation of carbides, and coarsening of grains and precipitates.

**Acknowledgements** This work is financially supported by the National Natural Science Foundation of China-Outstanding Young Scholars (No. 52325407), the National Natural Science Foundation of China (No. 51904187), the Open Project of State Key Laboratory of Advanced Special Steel and Shanghai Key Laboratory of Advanced Ferrometallurgy, Shanghai University (SKLASS 2022-06).

## Declarations

**Conflict of interest** The authors state that there are no conflicts of interest to disclose.

## References

- [1] A.Q. Zuo, X. Liu, C.D. Shao, M.Z. Fan, N.S. Ma, F.G. Lu, *Acta Metall. Sin. -Engl. Lett.* **35**, 1317 (2022)
- [2] G. Magudeeswaran, V. Balasubramanian, S. Sathyanarayanan, G.M. Reddy, A. Moitra, S. Venugopal, G. Sasikala, *J. Iron. Steel Res. Int.* **17**, 51 (2010)
- [3] Y. Li, S. Huang, H. Hui, Y.L. Han, J.Y. Huang, Z.P. Chen, *J. Mater. Sci.* **58**, 3802 (2023)
- [4] P. Tao, C. Zhang, Z.G. Yang, H. Takeda, *J. Iron. Steel Res. Int.* **17**, 74 (2010)
- [5] Q. Wang, C.D. Shao, H.C. Cui, Y. Gao, F.G. Lu, *Acta Metall. Sin. -Engl. Lett.* **35**, 714 (2022)
- [6] K. Ding, H.J. Hi, X. Liu, P. Wang, Q.L. Zhang, X.H. Li, Y.L. Zhao, *J. Iron. Steel Res. Int.* **25**, 847 (2018)
- [7] M.H.S. Bidabadi, Y. Zheng, A. Rehman, C. Zhang, H. Chen, P. Hou, Z.G. Yang, *J. Iron. Steel Res. Int.* **26**, 898 (2019)
- [8] X.Y. Li, Y. Jiang, K.F. Wu, W.L. Dong, F. Yang, X.W. Jia, X.L. Xu, J.H. Chen, R. Cao, *Int. J. Pres. Ves. Pip.* **193**, 10445 (2021)
- [9] Y.M. Li, Y.H. Cui, J.M. Zhang, M.H. Song, C. Xu, *Metals* **12**, 1978 (2022)
- [10] M.Y. Chai, M. Qin, Y.T. Zheng, X.L. Hou, Z.X. Zhang, G.X. Cheng, Q. Duan, *Mater. Today Proc.* **5**, 13759 (2018)
- [11] K. Ding, H.J. Ji, Q.L. Zhang, X. Liu, P. Wang, X.H. Li, L. Zhang, Y.L. Gao, *J. Iron. Steel Res. Int.* **25**, 839 (2018)
- [12] M.T. Ma, K.J. Li, Y. Si, P.J. Cao, H.Z. Lu, A.M. Guo, G.D. Wang, *Acta Metall. Sin. -Engl. Lett.* **36**, 1144 (2023)
- [13] Z.H. Jiang, P. Wang, D.Z. Li, Y.Y. Li, *Mater. Sci. Eng. A* **699**, 165 (2017)
- [14] Y.H. Li, Z.H. Jiang, Z.D. Yang, J.S. Zhu, *Acta Metall. Sin. -Engl. Lett.* **33**, 1346 (2020)
- [15] M.B. Wang, R.D. Li, T.C. Yuan, H.O. Yang, P.D. Niu, C. Chen, *Acta Metall. Sin. -Engl. Lett.* **35**, 354 (2022)
- [16] S.I. Rao, C. Woodward, B. Akdim, *Acta Mater.* **243**, 118440 (2023)
- [17] Y. Han, J.Q. Sun, J.P. Sun, G.Q. Zu, W.W. Zhu, W. Ran, *Acta Metall. Sin. -Engl. Lett.* **34**, 789 (2021)
- [18] Y.K. Mu, L.H. He, S.H. Deng, Y.F. Jia, Y.D. Jia, G. Wang, Q.J. Zhai, P.K. Liaw, C.T. Liu, *Acta Mater.* **232**, 117975 (2022)

Springer Nature or its licensor (e.g. a society or other partner) holds exclusive rights to this article under a publishing agreement with the author(s) or other rightsholder(s); author self-archiving of the accepted manuscript version of this article is solely governed by the terms of such publishing agreement and applicable law.